

Optical Properties Effects Upon the Collection Efficiency of Optical Fibers in Different Probe Configurations

Paulo R. Bargo, Scott A. Prah, and Steven L. Jacques

Abstract—When optical fibers are used for delivery and collection of light, two major factors affect the measurement of collected light: 1) light transport in the medium from the source to the detection fiber and 2) light coupling to the optical fiber (which depends on the angular distribution of photons entering the fiber). This paper studies the latter factor, describing how the efficiency of the coupling depends on the optical properties of the sample. The coupling dependence on optical properties is verified by comparing experimental data to a simple diffusion model and to a Monte Carlo (MC)-corrected diffusion model. Mean square errors were 7.9% and 1.4% between experiments and the diffusion, and experiments and the MC-corrected models, respectively. The efficiency of coupling was shown to be highly dependent on the numerical aperture (NA) of the optical fiber. However, for lower scattering, such as in soft tissues, the efficiency of coupling could vary two- and three-fold from that predicted by fiber NA. The collection efficiency can be used as a practical guide for choosing optical fiber-based systems for biomedical applications.

Index Terms—Collection efficiency, diffusion, light transport, Monte Carlo, optical fibers.

I. INTRODUCTION

OPTICAL fibers are an important tool for remote optical measurements and have been extensively used as light delivery and collection tools for optical diagnosis. They have been used in various configurations for the quantitative determination of chromophore concentration [1]–[3], tissue optical properties [4], [5], particle sizes [6], and to monitor pharmacokinetics [7]. Two major factors affect the measurement of collected light: 1) light transport from the source to the fiber and 2) light coupling into the optical fiber (which depends on the angular distribution of photons at the fiber face). Studies of how optical properties affect the intensity of light traveling through a medium have resulted in improved light transport models [8]–[12] but little work has been done on light coupling into an optical fiber. Some investigators consider the light coupling to an optical fiber to be part of the light transport model (e.g., including the optical fiber boundaries in Monte Carlo (MC) simulations [1], [4]) and do not separate these two factors. Two advantages of separating

Manuscript received November 20, 2002; revised February 3, 2003. This work was supported in part by the Collins Foundation and in part by the National Institute of Health under Grant no. EB00224. The work of P. R. Bargo was supported by Coordenação de Aperfeiçoamento de Pessoal de Ensino Superior, Brazilia, Brazil.

The authors are with the Providence St. Vincent Medical Center and with the Oregon Health & Science University, Portland, OR 97225 USA (e-mail: sjacques@ece.ogi.edu).

Digital Object Identifier 10.1109/JSTQE.2003.811287

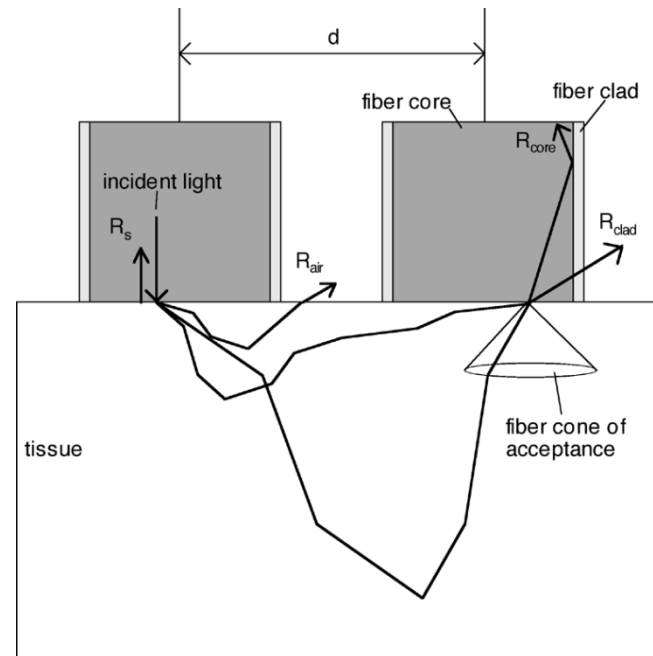


Fig. 1. Diagram of the possible return paths of light in a two-fiber configuration. Light that reaches the fiber face with an angle smaller than the half angle of the acceptance cone will be guided through the fiber to the detector (R_{core}). Light that reaches the fiber face with an angle greater than the half angle of the acceptance cone will escape through the fiber cladding (R_{clad}). R_{air} is the light that leaves the tissue outside the fiber and r_{sp} is the Fresnel reflection due to the fiber/tissue index of refraction mismatch. Light can also be absorbed by the tissue.

the light transport problem from the fiber-coupling problem are: 1) implementation of simpler models for light transport and 2) better understanding of the influences of the fiber on the detection scheme. The latter may guide the development of improved optical fiber-based systems.

We have previously demonstrated how the light coupling changes for different optical properties when a single optical fiber is used as source and detector [13] by determining the *optical fiber collection efficiency* (η_c) as a function of optical properties. The optical fiber collection efficiency was defined for a single optical fiber [13] as the fraction of light that couples to the optical fiber within the fiber's acceptance solid angle (R_{core}) divided by all the light that enters the fiber's face ($R_{\text{core}} + R_{\text{clad}}$) as illustrated in Fig. 1 and stated in (1)

$$\eta_c = \frac{R_{\text{core}}}{R_{\text{core}} + R_{\text{clad}}} \quad (1)$$

where R_{core} represents the light that enters the optical fiber core with an angle smaller than the fiber's half angle of acceptance [defined by the numerical aperture (NA)] and R_{clad} represents the light that enters the optical fiber core with an angle greater than the fiber's half angle of acceptance or enters the fiber clad with any angle; hence, this portion of the light defined by R_{clad} escapes through the fiber cladding and is not guided to the detector. The sum $R_{\text{core}} + R_{\text{clad}}$ accounts for all the light that enters the fiber face. The same definition of the collection efficiency can be used to multiple fiber configurations.

The parameter R_{core} can be determined by integrating the radiance [in $\text{W}/(\text{cm}^2\text{sr})$] within the solid angle of acceptance (Ω_a) and the fiber-core area (S_{core})

$$R_{\text{core}} = \int_{S_{\text{core}}} \int_{\Omega_a} L(\vec{r}, \vec{s}) d\Omega dS \quad (2)$$

where \mathbf{r} is the position in the medium and \mathbf{s} is the direction unit vector.

The total light that enters the fiber face is determined by integrating the radiance at the fiber face within a solid angle of 2π steradians. The collection efficiency will depend on the optical properties and on the probe geometry since the radiance probed by the optical fiber depends on the medium optical properties, the fiber position and the viewing direction. The average depth from which a photon takes its final unscattered step and escapes a highly scattering medium will be concentrated close to the fiber face when the mean free path ($\text{mfp} = 1/(\mu_a + \mu_s)$) is small in comparison to the fiber diameter. When the photons have been scattered many times, the angular distribution of the photons escaping the medium within the area of collection of the fiber will be nearly uniform events. In this case, the influence of the medium absorption coefficient and the geometry imposed by the source-detector fiber separation on the collection efficiency are minimal. However, in a low-scattering medium, the average depth from which a photon takes its final unscattered step and escapes the medium is much deeper in the medium. A greater number of escaping photons within the area of the collection fiber will escape with preferred angles (depending on the probe configuration), making the angular distribution of the escaping photons nonuniform. The fraction of escaping photons entering the fiber within the cone of collection will be strongly influenced by the number of scattering events and by the probe configuration.

Experimental measurements of the light transport for a fixed source-detector fiber separation are compared to models based on the diffusion approximation of the steady-state radiative transport with and without correction for the collection efficiency determined from MC simulations. These models will be designed MC-diffusion and diffusion, respectively. We demonstrate that, by accounting for the collection efficiency, the mean square error between model and experiment is reduced from 7.9% to 1.4% as the absorption coefficient varies from 0.1 to 5 cm^{-1} , and the reduced scattering coefficient varies from 4 to 17 cm^{-1} . The influence of parameters such as the probe configuration, the collection fiber diameter, the numerical aperture, anisotropy of scattering and launching configuration on the collection efficiency were also tested by MC simulations.

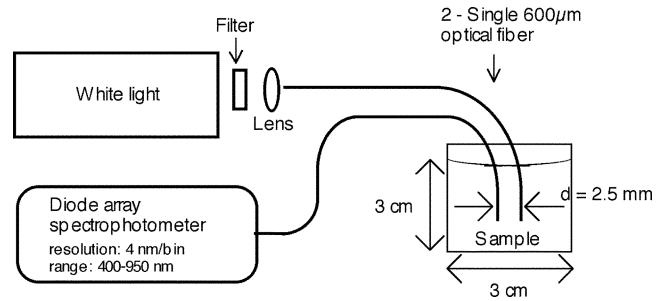


Fig. 2. Diagram of the experimental setup. A single 600- μm optical fiber is connected to a tungsten-halogen white lamp and the other is connected to a spectrophotometer. The space between the fibers is 2.5 mm. Fiber tips are aligned at the same depth 1.5 cm inside the sample. OD filters are used to avoid detector saturation.

II. MATERIAL AND METHODS

A. Optical Phantoms Preparation and Calibration

Optical phantoms were prepared using latex microspheres (5100B, 1.03- μm diameter, Duke Scientific, Palo Alto, CA) as scattering elements and India ink (no. 4415, Higgs, Lewisburg, TN) as the absorber. The absorption coefficient of the stock ink was determined with a UV-VIS spectrophotometer (model 8452A, Hewlett-Packard, Palo Alto, CA). The optical properties of the stock microspheres were determined by added-absorber spatially resolved steady-state diffuse reflectance measurements [14] as discussed in Appendix 1. Samples were prepared with microspheres concentrations of 8, 4, and 2% (μ'_s of 17, 8, and 4 cm^{-1} at 630 nm), forming three sets with seven samples for each concentration. Different aliquots of India ink were added resulting in final absorption coefficients at 630 nm of 0.1, 0.3, 0.7, 1.0, 2.0, and 5.0 cm^{-1} for each scattering set. The final sample volume was 40 mL held in a 3-cm diameter by 3-cm height container.

B. Reflectance Measurements and Analysis

Samples were measured by inserting two independent 600- μm optical fibers (FT600ET, Thorlabs, Newton, NJ), held by a fixed support with a separation distance of 2.5 mm between them, 1.5 cm below the surface inside the media. Fiber tips were carefully aligned to the same height. One fiber was connected to a tungsten-halogen white lamp (LS-1, Ocean Optics, Inc., Dunedin, FL) and the other to a spectrometer (S2000, Ocean Optics, Inc., Dunedin, FL) controlled by a laptop computer. The experimental setup is shown in Fig. 2. Acquisition time was 200 ms. Neutral density filters with one- or two-OD (03FNG057 and 03FNG065, Melles Griot, Irvine, CA) were used to avoid detector saturation. For each microsphere concentration, the experimental measurements were normalized by the measurement of the sample with the lowest absorption coefficient (0.1 cm^{-1}). Normalized data were compared to the normalized upward flux at the face of the fiber determined by [15]

$$F_{z-} = \frac{\phi(r)}{4} - \frac{F(r) \cdot \hat{z}}{2} \quad (3)$$

where $\phi(r)$ is the radial fluence rate and $F(r)$ is the net flux determine by

$$\phi(r) = \frac{\exp\left(-\frac{r}{\delta}\right)}{4\pi D r} \quad (4)$$

$$F(r) = -D\nabla\phi(r) = \frac{z_o}{4\pi} \left(\frac{1}{\delta} + \frac{1}{r_1}\right) \frac{\exp\left(-\frac{r_1}{\delta}\right)}{r_1^2} \quad (5)$$

where $z_o = 1/(\mu_a + \mu'_s)$, $D = z_o/3$, $\delta^2 = D/\mu_a$, and $r_1^2 = z_o^2 + r^2$. The reference depth ($z = 0$) was assumed to be the fiber face on this analysis. The diffusion upward flux was normalized by the upward flux obtained for the optical properties of the lowest absorption samples for each set of microspheres concentration. The normalized experimental flux was also compared with an MC-corrected diffusion equation (MC-diffusion model). For the MC-diffusion model, the collection efficiency (η_c) of the optical fiber obtained from MC simulations was used as a multiplicative correction factor on the diffusion model. The MC-diffusion model was normalized in the same way for comparison with the data.

C. MC Simulations

MC simulations were performed for a set of optical properties to establish η_c . The MC model was described elsewhere [13]. Briefly, photons $\geq 1\,000\,000$ were randomly launched uniformly within the radius of the fiber, forming a collimated beam into a homogenous medium. Proper boundary conditions were assigned depending on the medium being infinite or semi-infinite and the probe configuration being a single fiber, two fibers, or multiple fibers. Each photon was assigned a weight $1 - r_{sp}$, where r_{sp} is the specular reflectance at the fiber tip, prior to launching, and was propagated in the medium by steps with a random stepsize $d = -\ln(RND)/(\mu_a + \mu_s)$, where RND was a pseudorandom number uniformly distributed between zero and one. After every propagation step, the weight of the photon was multiplied by $(1 - a)$, where $a = \mu_s/(\mu_a + \mu_s)$. A new direction was chosen according to the Henyey–Greenstein scattering function [16], [17] in (6)

$$\cos(\theta) = \frac{1}{2g} \left[1 + g^2 - \left(\frac{1 - g^2}{1 - g + 2gRND} \right)^2 \right]. \quad (6)$$

The average cosine of the angle of photon deflection by a single scattering event (or anisotropy, g) was set to 0.83 for most runs. Different anisotropies were tested to evaluate the model dependence on this parameter.

If a photon crossed an air/sample boundary (in the semi-infinite case) with any escaping angle, then the variable R_{air} was incremented by a value $W(1 - r_i)$, where r_i is the internal specular reflection which varies with angle of escape according to Fresnel equations [(7), for unpolarized light] [18] and W was the photon weight at the moment of escape

$$R(\theta) = \frac{1}{2} \left[\frac{\sin^2(\theta_i - \theta_t)}{\sin^2(\theta_i + \theta_t)} + \frac{\tan^2(\theta_i - \theta_t)}{\tan^2(\theta_i + \theta_t)} \right]. \quad (7)$$

If the photon crossed a sample/fiber boundary with an escaping angle smaller than the half angle defined by the NA of the fiber (e.g., NA = 0.39), the escaping photon weight incremented the variable R_{core} . If the photon crossed a sample/fiber boundary with an escaping angle greater than the angle defined

by the NA of the fiber, the escaping photon weight incremented the variable R_{clad} . In the MC code, the size of optical fiber cladding was neglected for simplification. Escaping angles were corrected according to Snell's Law to account for the refractive index mismatched at the boundary. The photon was returned to the tissue with the remaining weight ($r_i W$) and continued propagating until being terminated according to the roulette method [19]–[21] to conserve energy. Values of η_c were determined by combining the values of the bins R_{core} and R_{clad} according to (1).

In the first experiment η_c was determined for a large range of optical properties with the same parameters of the experimental setup (two-fibers configuration in an infinite medium, fiber separation of 2.5 mm, fiber diameter 600 μm and NA of 0.39). In the second test, the two-fiber configuration in an infinite medium was compared to the two-fiber configuration in contact with a semi-infinite medium and with a multiple-fiber configuration in contact with a semi-infinite medium. The multiple-fiber configuration was implemented by a central source fiber surrounded by a ring of collection fibers. The other parameters were kept the same. The influence of the fiber separation was determined in a third experiment with the multiple-fiber configuration in contact with a semi-infinite medium. The distance between the source and collection fibers was varied from 0 to 5 mm. The condition for the separation equal to zero is equivalent to the special case of a single fiber used as source and detector. The fiber diameter was 600 μm and the NA was 0.39. A fourth experiment was done to evaluate the influence of the collection fiber diameter on η_c . For this test, the diameter of the source fiber was kept constant at 600 μm and the diameter of the collection fiber was varied from 100 μm to 2 mm. These tests were performed for the multiple-fiber configuration in contact with a semi-infinite medium and separation between the central fiber and the center of the ring of 2.5 mm. The NA was kept constant at 0.39. A fifth experiment was done to evaluate the influence of the numerical aperture on η_c . This experiment was performed for the multiple-fiber configuration in contact with a semi-infinite medium, with separation between the central fiber and the center of the ring of 2.5 mm and with source and collection fiber diameters of 600 μm . Simulations were also made to evaluate the influence of the anisotropy and the launching configuration in the source fiber. For all simulations the index of refraction of the sample (n_s) and fiber (n_f) were fixed at 1.335 and 1.458, respectively.

III. RESULTS

Fig. 3 shows the results for the normalized upward flux as a function of the absorption coefficient. Each cluster of three different symbols represents the normalized upward flux determined by experiment (\bullet), diffusion approximation (\diamond), and by the MC-diffusion model (\square). Measurements on three samples of the 3×6 matrix are shown with three wavelengths (532, 633, and 810 nm) for each sample. The reduced scattering coefficients at 633 nm were 4, 8, and 17 cm^{-1} (top to bottom). Error bars are shown for the experiment and for the MC-diffusion model as vertical lines. Mean square errors of 7.9 and 1.4% (with maximum errors up to 93 and 38%) were determined be-

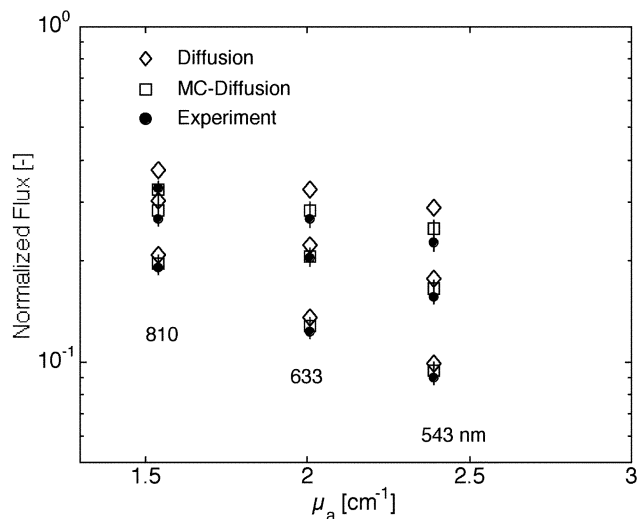


Fig. 3. Upward flux normalized by the flux for the lowest absorption sample as a function of the absorption coefficient. The reduced scattering coefficients at 633 nm were 4, 8, and 17 cm^{-1} (top to bottom). Vertical lines for the experiment and for the MC-diffusion model are the standard deviation of five measurements ($N_{\text{photons}} = 10^6$).

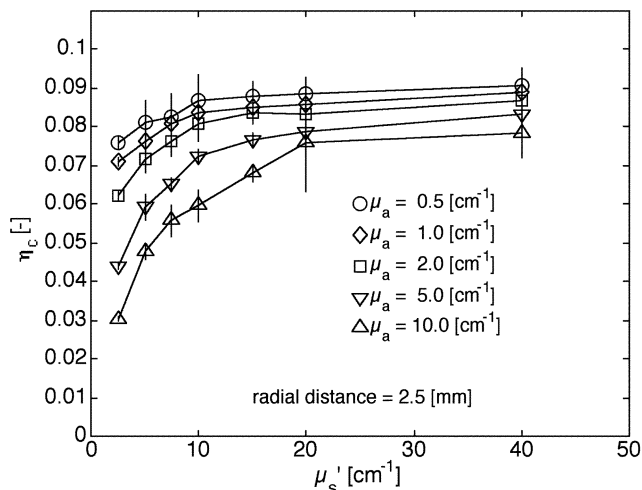


Fig. 4. Collection efficiency (η_c) determined by MC simulations plotted as a function of optical properties for the two-fibers configuration inserted to an infinite medium. These values were used to modify the diffusion model into the MC-diffusion model shown in Fig. 3. Error bars are the standard deviation of five MC runs with different random number seeds. The separation between the source and collection fibers was 2.5 mm, fiber diameters were 600 μm , and the NA was 0.39.

tween diffusion and experiment and between MC-diffusion and experiment, respectively.

Collection efficiencies for two fibers in an infinite medium with no boundary were determined by MC simulations and are shown in Fig. 4 for different optical properties. These values were used to modify the diffusion model into the MC-diffusion model shown in Fig. 3. Error bars are the standard deviation of five MC runs with different random number seeds and 1 000 000 photons launched per run. The separation between the source and collection fibers was 2.5 mm, fiber diameters were 600 μm , and the NA was 0.39.

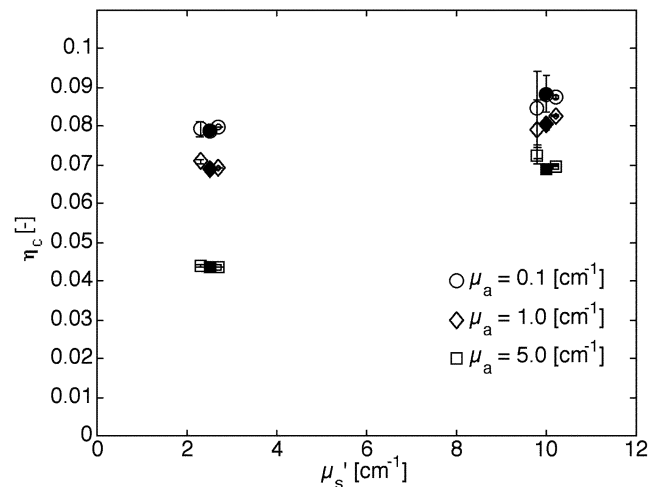


Fig. 5. Comparison between the collection efficiency determined by MC simulations for two fibers in contact to an infinite medium with no boundaries (empty symbols), two fibers in contact to a semi-infinite medium with an air/medium boundary (filled symbols), and a multiple-fiber probe with a central source fiber surrounded by an annular detection ring placed on the surface of a semi-infinite medium with air/medium boundary (doubled symbols). Data for the infinite medium configuration are plotted artificially skewed of -0.2 cm^{-1} and data for the multiple-fiber probe are plotted artificially skewed of $+0.2 \text{ cm}^{-1}$ to help visualization. Error bars are the standard deviation of five MC runs. The separation between the source and collection fibers was 2.5 mm, fiber diameters were 600 μm , and the NA was 0.39.

Similar data was obtained for two fibers placed on the surface of a semi-infinite medium with an air/medium boundary (filled symbols) and for a multiple-fiber probe with a central source fiber surrounded by an annular detection ring placed on the surface of a semi-infinite medium with air/medium boundary (doubled symbols). These configurations are compared to the two-fibers configuration in a infinite medium (empty symbols) in Fig. 5. Data for the infinite medium configuration are plotted artificially skewed of -0.2 cm^{-1} and data for the multiple fiber probe are plotted artificially skewed of $+0.2 \text{ cm}^{-1}$ to help visualization. Error bars are the standard deviation of five MC runs. The separation between the source and collection fibers was 2.5 mm, fiber diameters were 600 μm , and the NA was 0.39.

Collection efficiency as a function of optical fiber separation are shown in Fig. 6 for the multiple-fiber probe with a central source fiber surrounded by an annular detection ring placed on the surface of a semi-infinite medium with air/medium boundary. Fig. 6(a) is the special case of a single fiber used as source and detector. Drawings on top of the figures represent a front view of the face of the probes.

The influence of the diameter of the collection optical fiber on η_c was determined for the multiple-fiber probe configuration as shown in Fig. 7. The source fiber was kept with a diameter of 600 μm , separation between the source and collection fibers was 2.5 mm, and the NA was 0.39. Coincidentally, the values of η_c for μ_s' of 2.5 cm^{-1} and μ_a of 1 cm^{-1} (empty circles) overlap with the values obtained for μ_s' of 10 cm^{-1} and μ_a of 5 cm^{-1} (filled diamonds).

Fig. 8 shows the influence of the numerical aperture on η_c . The chosen NA for these experiments were those of commercial optical fibers (0.22, 0.39, and 0.48) [22]. The numerical

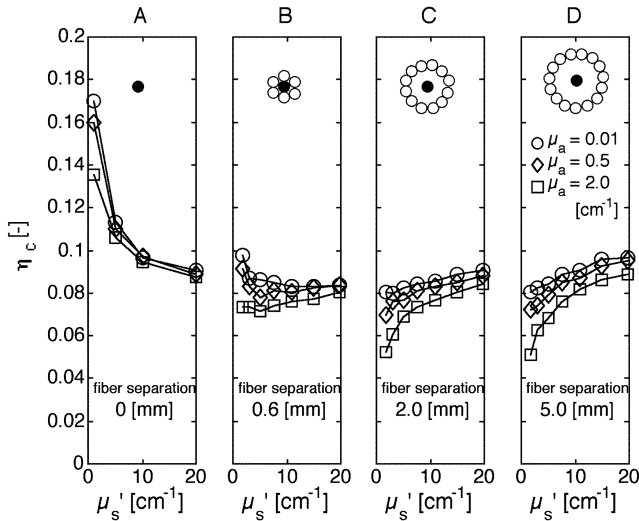


Fig. 6. Collection efficiency determined by MC simulations as a function of optical fiber separation for the multiple-fiber probe with a central source fiber surrounded by an annular detection ring placed on the surface of a semi-infinite medium with air/medium boundary. (A) is the special case of a single fiber used as source and detector. Drawings on top of the figures represent a front view of the face of the probes.

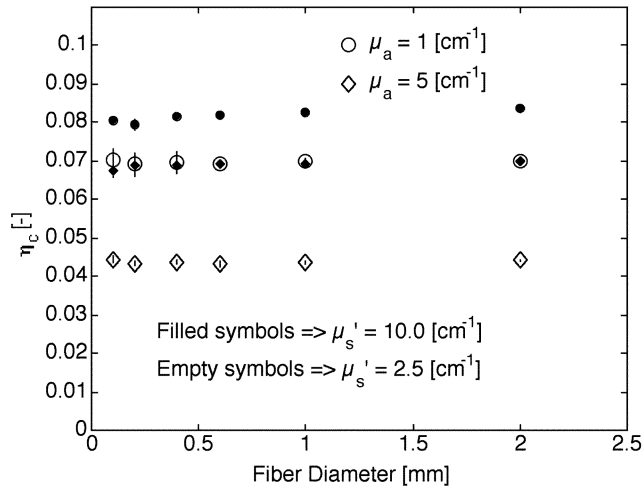


Fig. 7. Influence of the diameter of the collection optical fiber on η_c as determined for the multiple fiber probe configuration. The source fiber was kept with a diameter of $600 \mu\text{m}$, separation between the source and collection fibers was 2.5 mm , and the NA was 0.39 . Values of η_c for μ'_s of 2.5 cm^{-1} (empty symbols) and for μ'_s of 10 cm^{-1} (filled symbols) are shown. Error bars are the standard deviation of five MC runs and, in most cases, are smaller than the symbols.

apertures were corrected by the refractive index of the medium ($n_{\text{sample}} = 1.335$) to account for the effective cone of collection of the optical fiber. Dashed lines are the values obtained from (8) (in Section IV) for the corrected NAs. Values of η_c for μ'_s of 2.5 cm^{-1} and μ_a of 1 cm^{-1} (empty circles) coincidentally overlap with the values obtained for μ'_s of 10 cm^{-1} and μ_a of 5 cm^{-1} (filled diamonds).

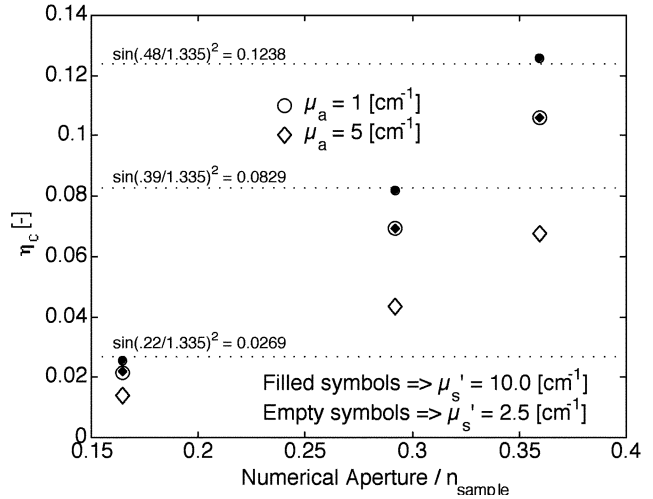


Fig. 8. Collection efficiency plotted as a function of numerical aperture of commercially available optical fibers ($\text{NA} = 0.22, 0.39, \text{ and } 0.48$). The numerical apertures were corrected by the refractive index of the medium ($n_{\text{sample}} = 1.335$) to account for the effective cone of collection of the optical fiber. Dashed lines are the values obtained from (8) (in Section IV) for the corrected NAs. Fiber diameter was $600 \mu\text{m}$ and fiber separation was 2.5 mm .

IV. DISCUSSION

The normalized upward flux in Fig. 3 showed that the MC-diffusion model predicted experimental values better than the diffusion model. The mean square error for the experimental versus diffusion model comparison was 7.9% and for the experimental versus MC, diffusion was 1.4% . For higher absorption coefficients, the square error can increase to as much as 93 and 38% for the diffusion and MC-diffusion comparison, respectively. Larger errors were observed for the measurements on the higher absorption samples for all sets of reduced scattering samples.

The parameter η_c (1) can be interpreted as the total fraction of light that couples into the optical fiber at an angle smaller than the acceptance angle defined by the fiber NA (θ_a), divided by the total light that enters the fiber face at all angles (8). We have demonstrated that η_c follows the form $\sin^2(\theta_a)$ for single fibers used simultaneously as source and detector [13].

$$\eta_c = \frac{R_{\text{core}}}{R_{\text{coll}}} = \frac{\int_0^{2\pi} d\phi \int_0^{\theta_a} \cos(\theta) \sin(\theta) d\theta}{\int_0^{2\pi} d\phi \int_0^{\pi/2} \cos(\theta) \sin(\theta) d\theta} = \frac{-\pi \sin^2(\theta) \Big|_0^{\theta_a}}{-\pi \sin^2(\theta) \Big|_0^{\pi/2}} = \sin^2(\theta_a) \quad (8)$$

For numerical apertures of 0.39 and a medium with index of refraction of 1.33 , θ_a equals 17° . Applying this angle in (8) gives η_c equal to 0.086 . The values of η_c calculated from (8) are a good first approximation for most optical properties (especially high-reduced scattering coefficients). But they do not agree for small values of μ'_s . In fact, η_c may vary as much as twofold when comparing data for low-reduced scattering with data for high reduced-scattering coefficients as observed in Fig. 4.

The cone of collection of an optical fiber (defined by the fiber NA) is dependent only on the indices of refraction of the fiber core/clad and the medium where the fiber is in contact [23]. Changes in the optical fiber collection efficiency for turbid media arises from differences in the angular distribution of the photons that reach the fiber for different optical properties. These changes are not caused by an intrinsic parameter of the optical fiber, but arise from its use in a turbid media, such as biological tissues. As a rule of thumb, the fraction of light collected by an optical fiber in a highly scattering medium can be approximated by the $\sin^2(\theta_a)$ rule determined for a single fiber used as source and detector. For multiple-fiber probes the $\sin^2(\theta_a)$ rule is not as accurate as for the single fiber case. This occurs because of the introduction of the extra geometrical parameter of the source detector fiber separation. The discrepancies become greater for increased absorption. For small-diameter single fibers the changes in absorption are less noticeable especially for high-reduced scattering coefficients due to the probing volume being very small so that the pathlength for absorption to exert its effect is short. There exist a transition in behavior of η_c as a function of the separation between source and detector as shown in Fig. 6. For large source detector separations the collection efficiency decreases for small-reduced scattering coefficients (by as much as twofold) and approach the value of $\sin^2(\theta_a)$ for high-reduced scattering coefficients [Fig. 6(c) and (d)]. For the very common probe with six fibers around one, η_c is less dependent on the reduced scattering coefficient [Fig. 6(b)]. For a single fiber used as source and detector, η_c behaves differently than for the case of two or more fibers with separation. In fact the opposite trend is obtained for low-reduced scattering coefficients and a twofold increase in η_c can be obtained.

No significant change in η_c was obtained when different multifiber probe geometries were tested as shown in Fig. 5. The influence of the diameter of the collection fiber on η_c was also negligible (Fig. 7). Fig. 8 shows that, independently of the optical fiber numerical aperture, η_c approaches the value of $\sin^2(\theta_a)$ for high-reduced scattering coefficients.

The effects of the anisotropy on the collection efficiency of the optical fiber are negligible as long as the reduced scattering coefficient remains the same and the anisotropy is close to one. We have tested the influence of the launching angle on the optical fiber collection efficiency (η_c) and have verified negligible effects. Keijzer *et al.* [24] showed that the fluence rate distribution is independent of the launching scheme. Our results for a single optical fiber confirm those obtained independently by Moffitt and Prah [4].

V. CONCLUSION

The parameter η_c is probably best implemented by an MC-generated lookup table to account for the coupling of light to the optical fiber since measurement of the light lost in the cladding is difficult. Knowledge of the optical property dependency of η_c can guide the choice of optical fiber systems to yield a η_c that is less sensitive to changes in the optical properties (e.g., changing the optical fiber diameter or the optical fiber NA). Also, the collection efficiency can

be used to understand differences between experimentally measured data and predicted values determined by models that do not account for the effects of the optical fiber coupling as shown in Fig. 3. Prediction of the collection efficiency for low-reduced scattering coefficients with the analytical formula (7) produced poor results highlighting the need for numerical models (e.g., MC simulations). The collection efficiency is an intrinsic problem for the usage of optical fibers in turbid media deriving from the fact that the angular distribution of the photons that return to the optical fiber is different for different optical properties. For highly scattering samples and a single optical fiber this distribution behaves as $\cos(\theta_a)\sin(\theta_a)$ and the amount of collected light behaves as $\sin^2(\theta_a)$. For multiple fiber configurations, the collection efficiency slightly deviates from this $\sin^2(\theta_a)$ rule and is particularly influenced by the absorption coefficient of the sample. Nevertheless, this rule of thumb provides a good estimate of the collection efficiency of the optical fiber when highly scattering samples are being measured. The collection efficiency behaves similarly for different multiple-fiber probe configurations. For a single fiber used as source and detector, the behavior of η_c is drastically changed. Negligible changes in η_c were observed for changes in the diameter or the numerical aperture of the collection fiber. The anisotropy of single scattering and the launching configuration had minimal effects on the collection efficiency. The parameter η_c can be used as a practical guide for choosing optical fiber-based systems for biomedical applications.

APPENDIX CALIBRATION OF SAMPLES

The optical properties of the samples were determined by added-absorber spatially resolved steady-state diffuse reflectance measurements [12]. Samples with high microsphere concentration (8%), no added absorber and low added-absorber were used in this experiment (0.1, 0.3, and 0.7 cm^{-1}). Two 400- μm -diameter optical fibers (FT400ET, Thorlabs, Newton, NJ) polished flat at both ends were inserted vertically side by side within the liquid samples to a depth of approximately half of its height (1.5 cm deep). The fiber faces were carefully aligned to the same depth and the fibers were pointing to the bottom of the container. One fiber was held fixed in the sample and was connected to a tungsten-halogen white lamp (LS-1, Ocean Optics, Inc., Dunedin, FL). The other fiber was held by a translation stage and connected to a diode array spectrophotometer (S2000, Ocean Optics, Inc., Dunedin, FL). The initial fiber separation was measured with a caliper (2.0 mm). The diffuse reflectance was measured at the initial fiber separation and for increasing fiber separations in four radial steps increments of 1.0 mm. The expected range of reduced scattering coefficients was determined by Mie scattering theory [25] to vary from approximately 20 down to 10 cm^{-1} across the visible spectrum of light (empty circles in Fig. 9). The samples were assumed to be homogeneous and infinite. Each set of 20 spectra [five fiber separations \times four samples (no ink and three increments in ink)] was fitted with a minimum square fitting routine to the solution of the steady-state diffusion equation [15] for an infinite medium. The sample with no added absorber

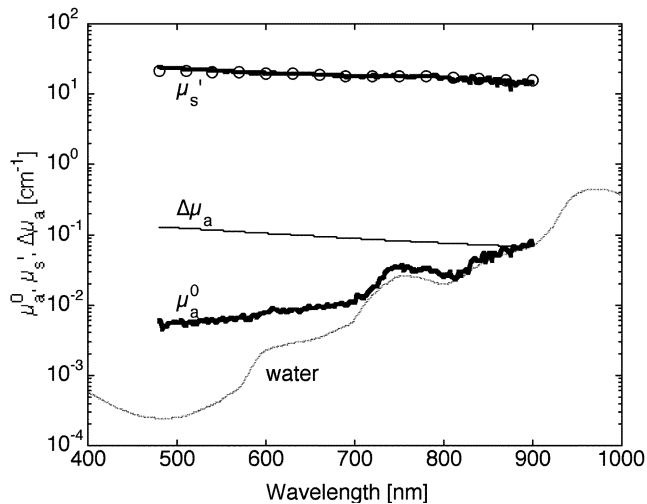


Fig. 9. Optical property spectra determined for the 1.03 μm diameter microspheres solution at a concentration of 8%. Absorption coefficients of water (dashed line) and the lowest ink aliquot are shown for comparison. Empty circles represent the reduced scattering coefficients determined by Mie theory for this sphere diameter.

had an absorption coefficient composed of just the baseline microspheres and water absorption coefficients (μ_a^0). The added absorber samples were assumed to have absorption coefficients composed of the μ_a^0 plus the added titrated ink absorption. All four samples were assumed to have the same reduced scattering coefficient (μ_s^0). The two fitting parameters were the reduced scattering coefficient and the baseline absorption coefficient for the original solution without ink. Values of 0.01 cm^{-1} and 20 cm^{-1} at 630 nm were determined for the absorption and reduced scattering coefficients, respectively. Results are shown in Fig. 9 along with the absorption coefficient of water (dashed line) and the absorption coefficient of the smallest aliquot of ink for comparison.

ACKNOWLEDGMENT

The authors would like to thank T. Moffitt and J. Ramella-Roman for their support and discussions.

REFERENCES

- [1] B. W. Pogue and G. Burke, "Fiber-optic bundle design for quantitative fluorescence measurement from tissue," *Appl. Opt.*, vol. 37, pp. 7429–7436, 1998.
- [2] S. L. Jacques *et al.*, "Reflectance spectroscopy with optical fiber devices and transcutaneous bilirubinometers," in *Biomedical Optical Instrumentation and Laser-Assisted Biotechnology*, A. M. V. Scheggi *et al.*, Eds., The Netherlands: Kluwer, 1996, pp. 83–94.
- [3] D. R. Braichotte, J. F. Savary, P. Monnier, and H. E. van den Bergh, "Optimizing light dosimetry in photodynamic therapy of early stage carcinomas of esophagus using fluorescence spectroscopy," *Laser Surg. Med.*, vol. 19, pp. 340–346, 1996.
- [4] T. P. Moffitt and S. A. Prah, "Sized-fiber reflectometry for measuring local optical properties," *IEEE J. Quantum Electron.*, vol. 7, pp. 952–958, 2001.
- [5] R. Bays, G. Wagnieres, D. Robert, D. Braichotte, J.-F. Savary, P. Monnier, and H. E. van den Bergh, "Clinical determination of tissue optical properties by endoscopic spatially resolved reflectometry," *Appl. Opt.*, vol. 35, pp. 1756–1766, 1996.

- [6] M. Canpolat and J. R. Mourant, "Particle size analysis of turbid media with a single optical fiber in contact with the medium to deliver and detect white light," *Appl. Opt.*, vol. 40, pp. 3792–3799, 2001.
- [7] D. R. Braichotte, G. A. Wagnieres, R. Bays, P. Monnier, and H. E. van den Bergh, "Clinical pharmacokinetic studies of photofrin by fluorescence spectroscopy in the oral cavity, the esophagus and the bronchi," *Cancer*, vol. 75, pp. 2768–2778, 1995.
- [8] S. L. Jacques, "Modeling light transport in tissue," in *Biomedical Optical Instrumentation and Laser-Assisted Biotechnology*, A. M. V. Scheggi, Ed., Dordrecht, The Netherlands: Kluwer, 1996, pp. 21–32.
- [9] M. Sinaasapel and H. J. C. M. Sternborg, "Quantification of the hematoporphyrin derivative by fluorescence measurement using dual-wavelength excitation and dual-wavelength detection," *Appl. Opt.*, vol. 32, pp. 541–548, 1993.
- [10] J. Wu, M. S. Feld, and R. P. Rava, "Analytical model for extracting intrinsic fluorescence in turbid media," *Appl. Opt.*, vol. 32, pp. 3585–3595, 1993.
- [11] C. M. Gardner, S. L. Jacques, and A. J. Welch, "Fluorescence spectroscopy of tissue: Recovery of intrinsic fluorescence from measured fluorescence," *Appl. Opt.*, vol. 35, pp. 1780–1792, 1996.
- [12] W. B. Pogue and T. Hasan, "Fluorophore quantitation in tissue-simulating media with confocal detection," *IEEE J. Quantum Electron.*, vol. 2, pp. 959–964, Dec. 1996.
- [13] P. R. Bargo, S. S. Prah, and S. L. Jacques, "Collection efficiency of a single optical fiber in turbid media," *Appl. Opt.*, vol. 42, pp. 1–11, 2003.
- [14] B. C. Wilson, "Measurement of tissue optical properties: Methods and theories," in *Optical-Thermal Response of Laser Irradiated Tissue*, A. J. Welch and M. J. C. van Gemert, Eds., New York: Plenum, 1995, pp. 233–274.
- [15] W. M. Star, "Diffusion theory of light transport," in *Optical-Thermal Response of Laser Irradiated Tissue*, A. J. Welch and M. J. C. van Gemert, Eds., New York: Plenum, 1995, pp. 131–206.
- [16] L. G. Henyey and J. L. Greenstein, "Diffuse radiation in the galaxy," *Astrophys. J.*, vol. 93, pp. 70–83, 1941.
- [17] A. N. Witt, "Multiple Scattering in Reflection Nebulae. I. A Monte Carlo Approach," *Astrophys. J.*, vol. 35, pp. 1–6, 1977.
- [18] E. Hecht, *Optics*, 4th ed. New York: Addison-Wesley, 2002, pp. 113–122.
- [19] L. Wang, S. L. Jacques, and L. Zheng, "MCML—Monte Carlo modeling of light transport in multi-layered tissues," *Comp. Meth. Prog. Biomed.*, vol. 47, pp. 131–146, 1995.
- [20] S. A. Prah and S. L. Jacques, Monte Carlo Simulations. [Online]. Available: <http://omlc.ogi.edu/software/mc/>
- [21] S. A. Prah, "Light transport in tissue," Ph.D. dissertation, Univ. of Texas, Austin, 1988.
- [22] Optical fiber catalog. CeramOptec Industries, Inc. [Online]. Available: <http://www.ceramoptec.com/>
- [23] M. Young, *Optics and Lasers: Including Fibers and Optical Waveguides*, 4th ed. New York: Springer-Verlag, 1992, pp. 250–252.
- [24] M. Keijzer, S. L. Jacques, S. A. Prah, and A. J. Welch, "Light distributions in artery tissue: Monte Carlo simulations for finite-diameter laser beams," *Lasers Surg. Med.*, vol. 9, pp. 148–154, 1989.
- [25] G. Mie, "Beiträge zur optik trüber medien speziell kolloidaler metallösungen," *Ann. Phys.*, vol. 25, pp. 307–445, 1908.



Paulo R. Bargo received the B.S. degree in electrical engineering from the National Institute of Telecommunications, Santa Rita do Sapucaí, Brazil, in 1992, the M.S. degree in electrical engineering from the University Vale do Paraíba, São José dos Campos, Brazil, in 1995, and is currently pursuing the Ph.D. degree in electrical engineering from the Oregon Health and Science University, Portland.

He was a visiting student at the G.R. Harrison Spectroscopy Laboratory, Massachusetts Institute of Technology, Cambridge, in 1996, and an Assistant

Professor at the University Vale do Paraíba during 1996–1998. His research interests include biomedical optics, photodynamic therapy, biomedical instrumentation, optical diagnostics, and spectroscopy.



Scott A. Prah received the B.S. degree in applied physics from the California Institute of Technology, Pasadena, in 1982, and the Ph.D. degree in biomedical engineering from the University of Texas, Austin, in 1988.

He is currently a Senior Scientist at the Oregon Medical Laser Center, Providence St. Vincent Medical Center, Portland. He is also an Assistant Professor of biomedical engineering in the OGI School of Science and Engineering, Oregon Health and Science University, Portland. His current research interests include photon migration, laser thrombolysis for stroke, molecularly imprinted polymers, and coagulation techniques for hemostasis during liver surgery.



Steven L. Jacques received the B.S. degree in biology and the M.S. degree in electrical engineering from the Massachusetts Institute of Technology, Cambridge, in 1975 and 1979, respectively, and the Ph.D. degree in biophysics and medical physics from the University of California, Berkeley, 1985.

He has been working in the field of biomedical optics and laser-tissue interactions for 19 years. He was with the Wellman Labs for Photomedicine, Massachusetts General Hospital, Boston, for five years and with the University of Texas M. D. Anderson Cancer Center, Houston, for eight years. For the past six years, he has been a Professor of biomedical engineering and a Research Associate Professor of dermatology at the Oregon Health and Science University, Portland, and a Senior Scientist at the Oregon Medical Laser Center, Providence St. Vincent Medical Center, Portland. His research has been funded by grants from the National Institute of Health, the National Science Foundation, the Department of Education, the Air Force Office of Scientific Research, and the Whitaker Foundation.